Global Doppler frequency shift detection with near-resonant interferometry

Andrin Landolt[1], Thomas Rösgen[2]

1: Institute of Fluid Dynamics, ETH, Zurich, Switzerland, landolt@ifd.mavt.ethz.ch
2: Institute of Fluid Dynamics, ETH, Zurich, Switzerland, roesgen@ifd.mavt.ethz.ch

Abstract A feasibility study about measuring 2D Doppler shifts using near-resonant interferometry is presented. In any interferometer with unequal optical path lengths, changes in frequency result in a phase shift and thus in a local distortion of the interference fringe pattern. By adding a dispersive element to one leg of an interferometer, the optical path length difference and hence the phase of the interference fringe pattern becomes strongly frequency dependent.

Using a DGV iodine vapor cell near a resonant transition as a dispersive medium, the system sensitivity is predicted. The dispersion of iodine near resonance is calculated from available absorption data trough optical data inversion with the Kramers-Kronig relations. From the variation of vapor pressure and temperature in the calculations, operating conditions for improved system sensitivity are derived.

Rotating disc experiments and measurements on a free jet with a pulsed laser light source show the applicability of the proposed method for planar Doppler measurements. The phase of a recorded fringe pattern is retrieved by quadrature filtering the recorded image and subsequently solving the phase-unwrapping problem in a least-squares sense. By subtracting the zero-velocity reference phase from the measured phase distribution, the local phase distortion due to the Doppler shift is computed.

The theoretical data is found to be in good qualitative agreement with the experimental measurements while quantitatively the system sensitivity is slightly overestimated by the theory. For the present setup, a spatial resolution of 10 pixels and a measurement error of a few m/s are estimated.

1. Introduction

The measurement of flow velocity distributions based on optical Doppler shift detection remains an active field of interest. By measuring the frequency shift of the light scattered off moving particles, one component of the flow velocity can be calculated. Without the need for resolving individual particles, such a method is particularly suited for large-scale applications or when seeding is difficult.

Doppler Global Velocimetry (DGV) was first presented by Komine et al. (1991). Using a narrow-band light source tuned onto the edge of an absorption filter, frequency shift is converted to intensity images. The technique has been developed since by various research groups and was successfully applied in full scale wind tunnels, high-speed flows and combustion measurements.

An alternative approach using Michelson interferometry to record so-called Doppler velocimetry pictures (DPV) was presented by Seiler et al. (1983; 1999). Due to a difference in optical path length of the interferometer caused by an inserted glass block, changes in frequency result in a phase shift and hence in a local distortion of the interference fringe pattern. The authors demonstrated the application of the method in various experiments.

We propose to measure global Doppler frequency shifts by placing a dispersive element in an interferometric setup. The optical path length difference between the two legs of the interferometer thereby becomes a strong function of frequency. Measurement sensitivity and non-linearity of the method can be controlled by the choice of the dispersive medium and the geometrical path length difference.

A possible dispersive medium is a molecular or atomic absorption filter near a resonant transition, where not only the transmission but also the refractive index become a function of

frequency. Primarily a function of temperature and number density, this capability is used in near-resonant holographic interferometry for concentration measurements (e.g. McIntyre et al. 2003). The accurate dispersion data, required to predict the characteristics of such a setup are scarce in the literature, whereas absorption data is often available. Fortunately, the refractive index can usually be calculated through optical data inversion of the absorption coefficient using the Kramers-Kronig relationships (Peiponen et al. 1998).

In the present study, the feasibility of measuring global Doppler shifts using near-resonant interferometry with a standard DGV iodine vapor cell near resonance is demonstrated. From the transmission profile predicted by Forkey et al. (1997), the theoretical system sensitivity is calculated and operating conditions of the cell for improved system sensitivity are derived. Rotating disc and free jet experiments demonstrate the applicability of the technique for planar Doppler shift measurements. The theoretical values are compared with good qualitative agreement to the experimental data.

2. Prediction of system performance

The phase difference $\Delta\phi$ of two light waves in the image plane of an interferometer is a function of the optical path difference, the angular frequency of the light ω and the speed of light c. With a dispersive element in one leg of the interferometer (Fig. 1), the optical path length difference becomes a function of frequency. The measurement sensitivity can be defined as the phase shift of the interference pattern due to a change in frequency:

$$\frac{\partial\Delta\phi}{\partial\omega} = \frac{2l}{c}\left[\omega\frac{\partial(n-1)}{\partial\omega} + (n-1)\right] + \frac{2L}{c}, \qquad (1)$$

where l is the length of the dispersive element, n its frequency-dependent refractive index and L the geometrical path difference. The system sensitivity is composed of a frequency dependent dispersive part and a term which only depends on the optical path length difference between the two interferometer arms.

In the vicinity of a resonant transition, the optical properties of a medium are characterized by a change in absorption and an associated region of dispersion, where the refractive index varies with wavelength. The relationship between absorption and dispersion, intrinsically linked with each other, can be described by the Kramers-Kronig relationships (Peiponen et al. 1998). From a known absorption coefficient, the refractive index can thus be obtained through the comparatively simple process of optical data inversion.

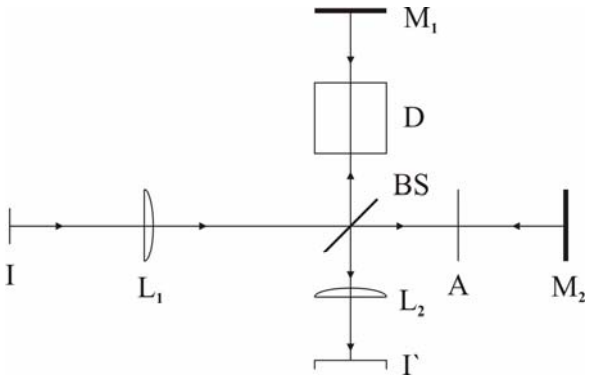

Fig. 1 Michelson interferometer with a dispersive element D. M_1 and M_2 are mirrors, BS the beam splitter and A an attenuator. The lenses L_1 and L_2 form an image of the object plane I on both mirrors and in the image plane I`.

The optical properties of iodine vapor, used as a dispersive medium for the present study, are

calculated with the absorption model proposed by Forkey et al. (1997). The shapes of the absorption lines are modeled therein as Gaussians, neglecting all inhomogeneous contributions. This approximation affects mainly the tails of the lines and differences between model predictions and experimental data arise at higher vapor pressures (Forkey et al. 1997). The effect of non-resonant background absorption, not included in Forkey`s code, was calculated directly from the constants tabulated by Tellinghuisen (1982).

Fig. 2 shows the transmissivity, the absorption coefficient, the refractive index and the system sensitivity for the iodine vapor cell used. From the plot, the strongest absorption line is identified as no. 1111 at a wavenumber of approximately 18788.45 cm^{-1} (Gerstenkorn and Luc 1978). The maximum gradient of refractive index is found on the blue side (high-frequency positive slope) of this line.

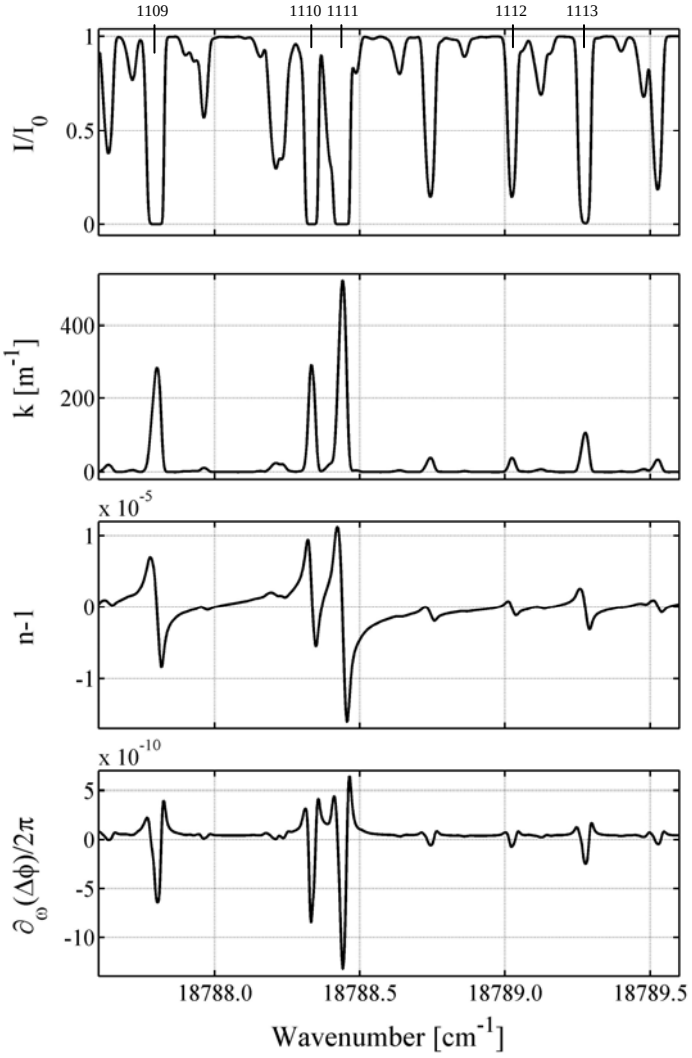

Fig. 2 Predicted iodine transmissivity, absorption coefficient, refractive index and system sensitivity for the iodine cell used. Line numbering according to Gerstenkorn and Luc (1978).

Calculations for varying vapor pressures show a proportional behavior of both absorption coefficient and gradient of refractive index with pressure (Fig. 3). In other words, doubling the cell length is equivalent in terms of sensitivity to doubling the vapor pressure. Consequently, the derivative of the refractive index normalized by the absorption coefficient is independent of the vapor pressure. Fig. 4 suggests that by finding a suitable combination of cell length and vapor pressure, a significant increase in system sensitivity can be achieved when moving away from the line centre. From the trend of the dashed line which neglects background absorption follows, that

the decrease around a wavenumber of 18788.49 cm^{-1} can be attributed to the weak line on the high-frequency edge of line no. 1111. The strong background absorption of iodine vapor at these particular wavelengths prevents an increase of this curve still further away from line center. The neglected pressure broadening (i.e. due to the deviation from the Gaussian line shape) possibly puts a limit on the system sensitivity away from line center as well. For different cell temperatures, the transmission and the derivative of the refractive index are shown in Fig. 5. Measurement sensitivity is slightly reduced at higher cell temperatures.

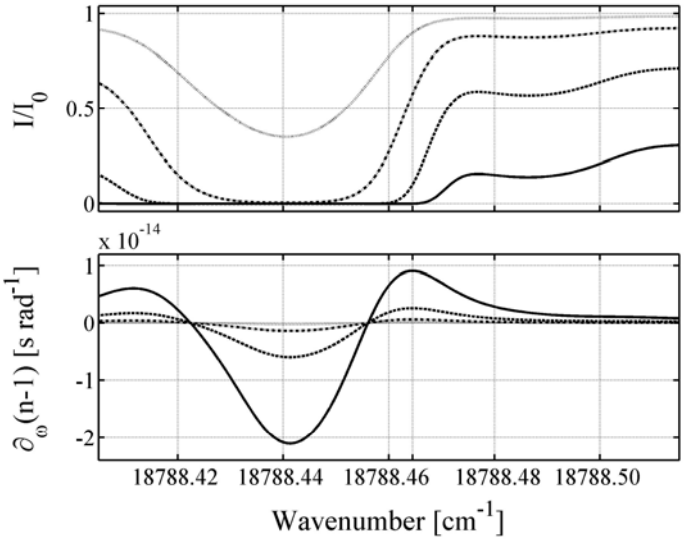

Fig. 3 Cell transmission and respective gradient of refractive index for line no.1111 at vapor pressures of 0.20, 1.03, 4.26 and 14.93 Torr and 100 °C cell temperature, including background absorption.

Fig. 6 illustrates the different characteristics of DGV, DPV and the proposed dispersive technique based on the iodine vapor cell used for this study. The sensitivity criterion for the ratio-based DGV technique can be defined as steepness of the filter in fractional transmission per unit frequency $\partial_\omega I/I_0$. For the interferometric DPV setup, the sensitivity is calculated based on an optical path length difference of 1.5 times the iodine cell length.

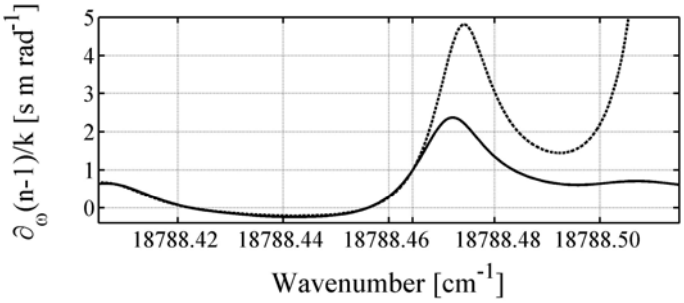

Fig. 4 Gradient of the refractive index divided by the absorption coefficient and normalized to the values for maximum gradient. The dashed line is without background absorption.

The sensitivity for both DGV and the presented technique reaches a maximum at approx. $6 \cdot 10^{-10}$ at nearly identical frequencies. A frequency shift of 1 MHz results in a 0.4% change in intensity or 2π phase shift, respectively. The peaks are significantly narrower for ratio techniques and reach quickly a value near zero, thus limiting the dynamic range. The comparatively slow decay for the dispersion technique, in combination with a DC component due to the non-zero optical path length difference, allows for large frequency shifts away from the line centre. The Doppler picture setup produces a frequency independent sensitivity of about 0.2 times the maximum for the dispersion

technique. It should be noted here that the sensitivity values can not be related directly to measurement accuracy. Hardware characteristics as well as post processing steps play an important role and need to be considered carefully.

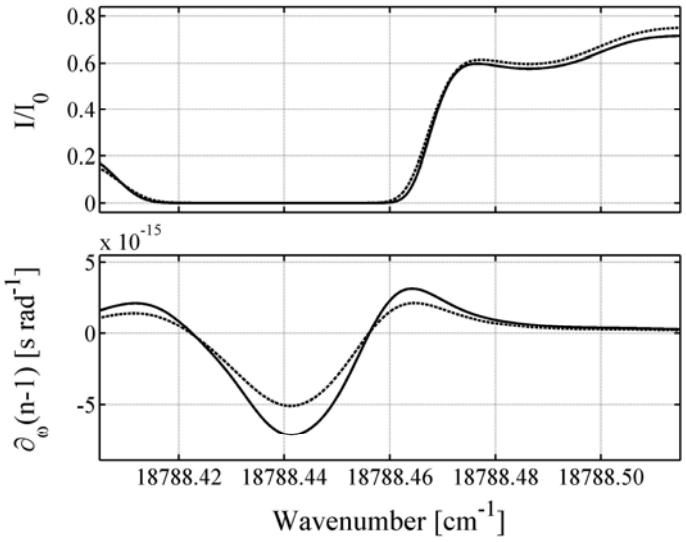

Fig. 5 Cell transmission and respective gradient of refractive index for line no. 1111 at cell temperatures of 70 (—) and 130 °C (- -) and 4.26 Torr vapor pressure, including background absorption.

3. Experimental Setup and Data Processing

The interferometer is assembled from 2" optics according to Fig. 1. An entry lens forms an image on both mirrors. The optical paths are recombined in the beam splitter and focused by a second lens to form an interference pattern on the image plane of the sensor of a PULNIX TM-1010 monochrome 10-bit camera synchronized with the laser. To increase the fringes' depth of modulation, the intensity of the two beams is matched by an attenuator. Fringe spacing and orientation are adjusted by tilting one of the mirrors. To limit the influence of vibrations or density variations along the optical path on the measurements, the interferometer is integrated into a single component with sealed arms as shown in Fig. 7.

As dispersive element a constant-density iodine vapor cell as described by Röhle (1999), originally designed for DGV applications is used. The cell with a length of 0.05 m and a diameter of 0.04 m has been filled at 60 °C resulting in a vapor pressure of 4.26 Torr. The stem temperature was set to 68 °C in the experiments. Cell and associated temperature controller were purchased from the German Aerospace Research Establishment (DLR) in Cologne. To verify the vapor pressure in the cell, the measured transmission profile was compared to the data provided by Forkey et al. (1997). Because of its smaller transmission, the left line in the line-group shown in Fig. 8 is sensitive to the vapor pressure and its depth allows to draw conclusions on the actual value (Fischer et al. 2000). The measurements were performed with a standard two-camera DGV setup, recording the filtered and the reference intensity of the light scattered off a stationary target while sweeping the laser through the frequency range of interest (Bömmels and Rösgen 2001). Transmission was subsequently obtained from the local normalized intensity ratio of the two images. As can be seen in Fig. 8, the measured transmission agrees well with the prediction.

The light source is a frequency-doubled injection-seeded long-pulse Nd:YAG laser. The system is a customized Shurelite PIV laser from Continuum with increased cavity length. Inherent to such systems are a long-term drift and pulse-to-pulse variations in frequency and power. This puts a limit on the accuracy of a direct system calibration (Meyers et al. 2001). In the present study, the laser frequency could not be monitored independently. For a detailed description of the laser system refer

to Bömmels and Rösgen (2001).

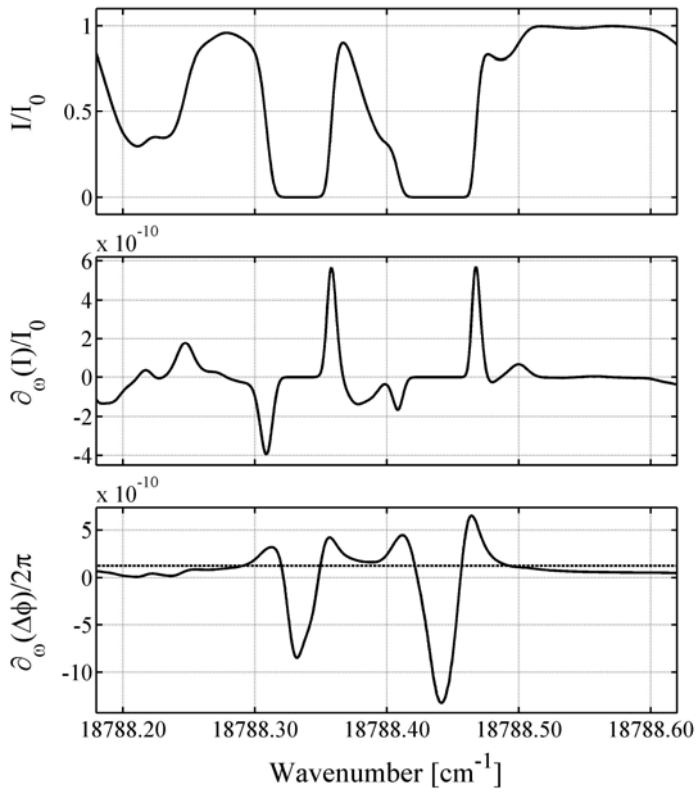

Fig. 6 Normalized transmission, gradient of normalized transmission and gradient of phase angle for the considered iodine vapor cell. The dashed line shows the behavior of a setup using a glass block of the same length.

The rotating disc with a diameter of 0.12 m is mounted in a frame which acts as a zero-velocity reference. Both are made of sand-blasted aluminum, imitating the scattering of a dense particle cloud. To illuminate disc and frame, the laser beam was radially expanded through a lens system. Rotational speed was set to 15'000 rpm and measured independently directly prior to recording an image. Before and after each measurement, 5 pictures of the stationary disc were taken to give an averaged zero-velocity reference fringe pattern. Fig. 7 shows the geometrical setup with the angle α set to 158° and β to 54.5°. $\underline{V}$ is the velocity vector, $\underline{l}$ the propagating direction of light and $\underline{o}$ the direction of observation. The distance between disc and entry lens was 0.85 m. All components were arranged in-plane.

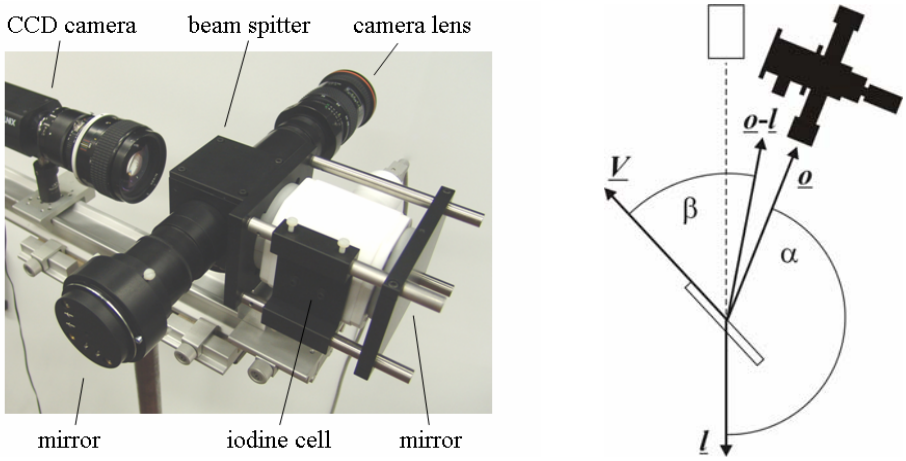

Fig. 7 Interferometric experimental setup and geometrical conditions.

For the subsonic jet experiments, pressurized air seeded with fog from a commercially available fog generator was expanded into the plenum trough a circular 0.017 m diameter nozzle. The exit speed was 110 m/s. A light sheet formed by a lens system illuminated the flow along its center line with the propagation direction of light directly opposed to the flow velocity. The interferometer was placed at a distance of 1.8 m from the nozzle and at an angle of 30° to the center line (α=150° and β=15°). To provide the necessary reference fringe pattern for a zero-velocity reference, images of a white surface placed in front of the nozzle were recorded prior to a measurement.

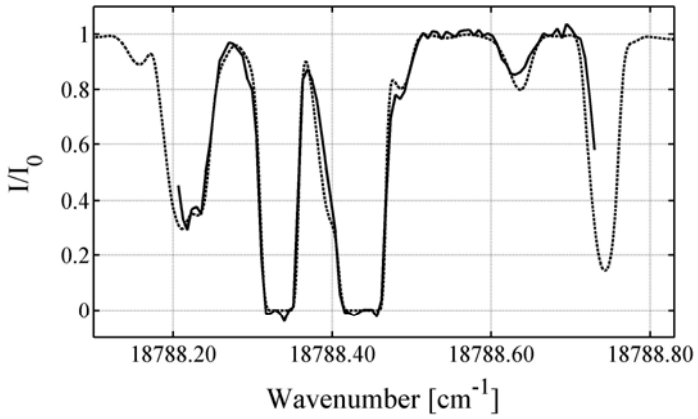

Fig. 8 Comparison of the predicted (dashed line) and the measured transmission profiles for the iodine cell used.

Both measurement and zero-velocity images undergo the same processing. The real and imaginary part of the local phase angle is retrieved by convolving the image with Gaussian-shaped quadrature filters which preserve the dominant spatial frequencies of the fringe pattern (Jähne 2005). Computation of the inverse tangent with the two images from the filtering yields the wrapped 2D phase. The phase unwrapping problem is then solved in a least-squares sense by using fast cosine transforms as suggested by Ghiglia et al. (1994). The local distortion of the phase angle due to Doppler shifts is finally computed by subtracting the zero-velocity reference from the measurement phase. In the present work, an unweighted approach for the phase unwrapping was used. The standard size of the Gaussian FWHM was 50 pixels. Filtering and computation of the unwrapped phase from one fringe pattern image takes about 30 s on a current workstation. The zero-velocity reference phase was computed from an average of 5 processed images. For simplicity, direction of observation and direction of light are assumed to be constant over the image. Image distortion as well as temporal and spatial variations of the laser frequency are not corrected for.

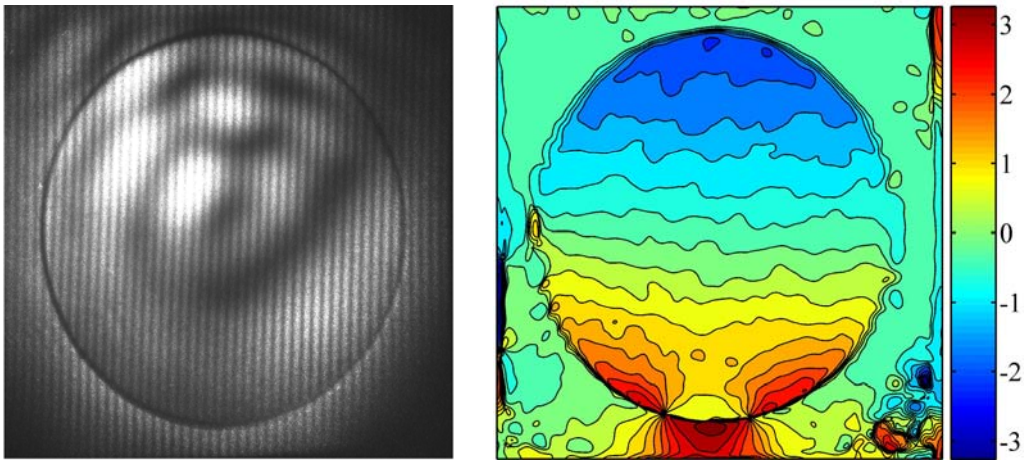

Fig. 9 Fringe pattern and net unwrapped phase shift for the rotating disc experiment. Phase angles given in rad.

3. Results

Fig. 9 shows a typical measurement image and the corresponding 2D phase shift angle computed from a single image. Other than by the quadrature filtering, no additional averaging is performed. The expected quasi-linear distribution of the phase shift along the vertical axis of the disc and the zero-phase shift for the stationary area outside the disc are accurately reproduced. In regions of low fringe contrast and at the edge of the disc the phase unwrapping becomes erroneous. The measurement of the phase shift at the lower end of the disc is difficult because frequency is shifted close to the line center to regions with high absorption.

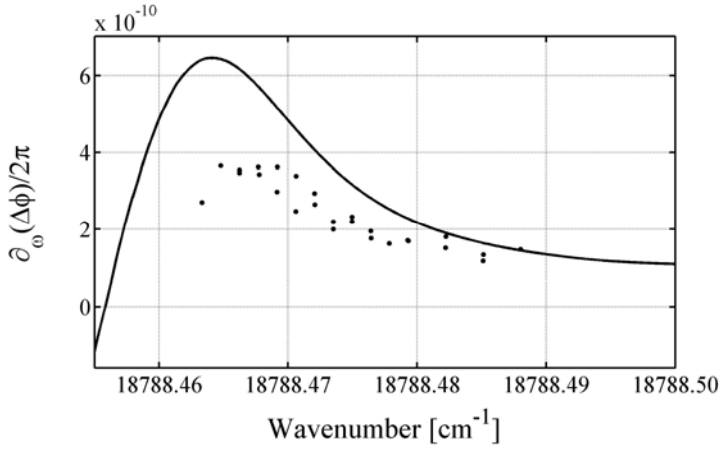

Fig. 10 Measured (symbols) and predicted (solid line) system sensitivity.

From measurements at different laser frequencies, the measurement sensitivity is computed based on the spatially averaged gradient of the phase shift near the disc center. The corresponding frequency shift is derived from disc speed, offset from disc center and the calculated Doppler shift (Fig. 10). The comparison of the measured values with the theoretical data confirms the predicted characteristics of system sensitivity. The magnitude of the system sensitivity appears to be overestimated by a factor of 1.5.

The influence of the fringe spacing on the standard deviation s of the measured phase angle is shown in Fig. 11. The standard deviation is computed from the unwrapped phase of 5 consecutive images in a region with good fringe contrast. The size of the quadrature filters remained unchanged. The fringe spacing is derived from the dominant spatial frequencies of the interference pattern. A distinct minimum at fringe spacing of 10 pixels is apparent.

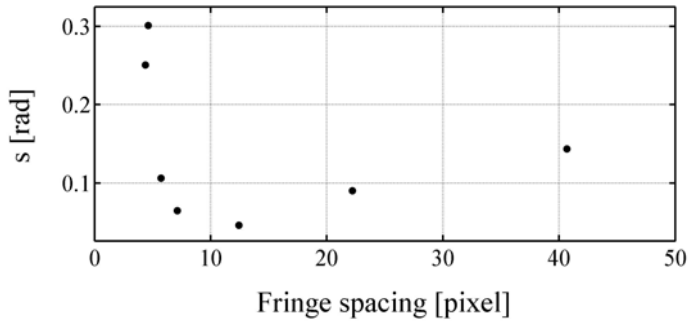

Fig. 11 Standard deviation s of single measurement images for different fringe spacing.

The computed phase shift angle along the vertical disc axis for varying filter sizes is shown in

Fig. 12. The fringe spacing was held constant. Due to the heavier spatial filtering, the curves are smoothed with increased filter size. Interestingly, the steepness of the phase jump at the edge of the disc is not strongly affected.

Fig. 13 shows both measurement image and phase shift for the free jet computed from a single image. Regions outside the seeded flow are set to zero using the measured image intensity as criterion. The typical flow topology of a free jet is clearly visible.

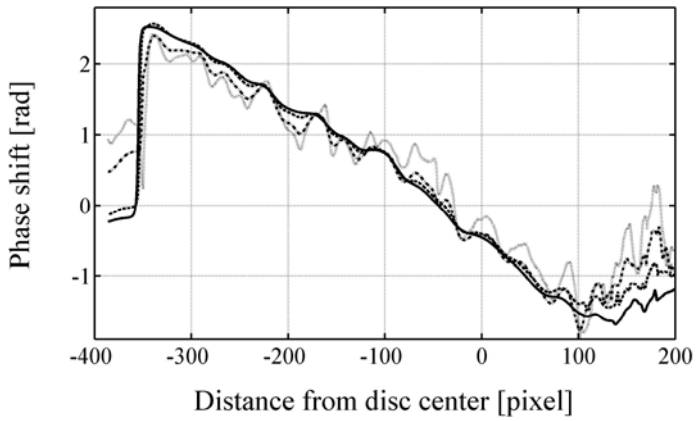

Fig. 12 Phase shift along the vertical disc axis computed with a filter size of 25 (··), 50 (-·), 100 (- -) and 150 (—) pixels.

3. Discussion

The results show that near-resonant interferometry is capable of measuring planar Doppler shifts. With theoretical absorption data, the main characteristics of the method can be predicted. The discrepancy between calculated and measured system sensitivity is most likely due to neglected pressure broadening processes in Forkey's model. The Lorentzian shape of inhomogeneous broadened lines with its more pronounced tails would lower the slope of the refractive index and hence the system sensitivity. Part of the difference could also be due to an overestimation of the vapor pressure in the iodine cell. The relatively poor temporal frequency stability of the laser system limits the accuracy of the cell calibration as well.

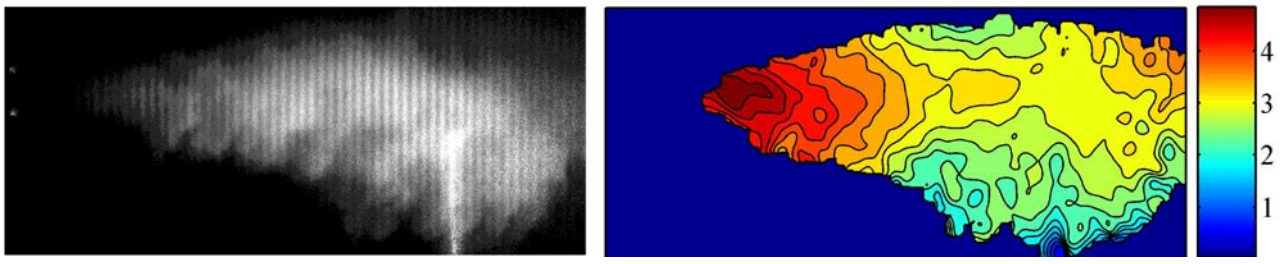

Fig. 13 Fringe pattern and net unwrapped phase shift for the free jet experiment. Flow from left to right, phase angles given in rad.

Poor frequency stabilization of the laser is probably the main reason for the scatter of the measurement points in Fig. 10. The images were recorded over a period of 1 hour and long-term drift of the laser is no longer negligible. The encapsulated design of the interferometer is found to eliminate the errors due to vibrations or density variations in the optical path almost completely.

The implemented post processing of the fringe images is comparatively robust and fast. Other approaches based on regularized phase-tracking proved to be less effective. Obvious problems arise in the vicinity of discontinuities (e.g. on the edge of the disc) or in regions with low fringe contrast.

Using a weighted approach for the phase unwrapping should help resolve both issues.

The experiments suggest a fringe spacing and a corresponding maximum spatial resolution of the technique of 7 to 15 pixel. Sub-pixel interpolation, not implemented in any of the processing steps so far, should allow for even smaller fringe spacings. Increasing the size of the quadrature filter decreases the measurement noise but simultaneously the spatial resolution. Because the reproduction of the disc edge does not seem to suffer excessively from increased filter size, a closer investigation of its influence is ongoing.

3. Conclusions

In the present study, the feasibility of measuring Doppler shifts with near-resonant interferometry could be demonstrated. Using a standard DGV iodine vapor cell as dispersive medium, the characteristics of the setup were predicted. The refractive index of iodine was calculated from theoretical absorption data trough optical data inversion. The main system characteristics were confirmed experimentally on a rotating disc while the capability of the method for 2D flow measurements was demonstrated in a free jet experiment.

The proposed method is inherently a single camera technique without the image alignment and camera calibration requirements of DGV. Because only the position of interference fringes has to be determined in the post processing step, camera image intensity noise affects measurement accuracy only in a minor way. The measurement range is much larger than for transmission based techniques, where it is restricted to the shoulder of one absorption line.

Although the post processing was not specifically adapted to the measurements, the quadrature filtering and the least-squares phase unwrapping proved to be fast and robust. Sub-pixel interpolation in the filtering step and a weighted approach for the phase unwrapping should reduce measurement error and increase spatial resolution significantly. The interaction of fringe spacing and filter size needs further investigation to define optimal parameters.

The experiments suggest a spatial resolution of 10 pixels and an accuracy of a few m/s for the present setup. The pulsed light source did not permit an accurate system calibration and hence estimates of the accuracy and uncertainty are based on the standard deviation of the measurements. A careful system calibration with a stable cw light source and including inhomogeneous broadening in the iodine absorption model will permit a better system characterization.

Measurement sensitivity and non-linearity of the method can be controlled by the choice of the dispersive medium and by choosing the geometrical path length difference. On a vapor cell specifically designed for near-resonant interferometry, the windows should be replaced by a beam splitter and a mirror which would reduce both the optical losses and the size of the system. The theoretical dispersion of iodine suggests moving away from the line center while increasing the optical depth to maximize the sensitivity. Regions of low background absorption and clear of weak transitions should be chosen. The use of dispersive media other than iodine should be investigated. This choice between numerous dispersive media such as molecular and atomic gas cells or Stark and Faraday effect filters, and the many ways to influence their dispersive properties, creates a highly adaptable technique.

References

Bömmels R, Rösgen T (2001) Development of a planar three-component velocimeter using Doppler Global Velocimetry (DGV) and PIV. In: 19th Int. Congress on Instrumentation for Use in Aerospace Simulation Facilities, Cleveland

Forkey JN, Lempert WR, Miles RB (1997) Corrected and calibrated I_2 absorption model at frequency-doubled Nd:YAG laser wavelentghs. Appl. Opt. 36(27):6729-6738

Gerstenkorn S, Luc P (1978) Atlas du spectre d'Absorption de la Molecule d'Iode, 14800-20000 cm^{-1}. Laboratoire Aimé-Cotton CNRS II, Orsay

Ghiglia DC, Romero LA (1994) Robust two-dimesional weighted and unweighted phase unwrapping that uses fast transforms and iterative methods. J. Opt. Soc. Am. A 11(1):107-117

Jähne B (2005) Digital image processing. 6. rev. and extended ed. Springer

Komine H, Brosnan SJ, Litton AB, Stappaerts EA (1991) Real-time Doppler Global Velocimetry. In: AIAA 29th Aerospace Sciences Meeting, Reno, paper 91-0337

McIntyre TJ, Bishop AI, Eichmann TN, Rubinsztein-Dunlop H (2003) Enhanced flow visualization with near-resonant holographic interferometry. Appl. Opt. 42(22):4445-4451

Meyers JF, Lee JW, Schwartz RJ (2001) Characterization of measurement error sources in Doppler global velocimetry. Meas. Sci. Technol. 12:357-368

Peiponen KE, Vartiainen EM, Asakura (1998) Dispersion, Complex Analysis and Optical Spectroscopy. Springer

Röhle I (1999) Laser-Doppler Velocimetry auf der Basis frequenzselektiver Absorption: Aufbau und Einsatz eines Doppler Global Velocimeters. DLR Forschungsbericht

Seiler F, Oertel H (1983) Visualization of velocity fields with Doppler-pictures. In: 3rd Int. Symp. on Flow Visualization, Ann Arbor

Seiler F, George A, Leopold F, Srulijes J, Smeets G (1999) Flow velocities visualization using Doppler picture interference velocimetry. In: ICIASF, Toulouse

Tellinghuisen J (1982) Transition strengths in the visible-infrared absorption spectrum of I_2. J. Chem. Phys 76(10):4736-4744